RSC Advances

PAPER

Cite this: *RSC Adv.*, 2023, **13**, 30520

Bi/BiOI/carbon quantum dots nano-sheets with superior photocatalysis†

Chenhui Zhao,[a] Zhijie Zhao,[a] Ying Liang[b] and Jiangfeng Fu*[a]

Received 30th July 2023
Accepted 7th October 2023

DOI: 10.1039/d3ra05145e

rsc.li/rsc-advances

A new photocatalyst of Bi/BiOI/Carbon quantum dots (CQDs) was synthesized *via* a simple method. Photocatalytic performance of Bi/BiOI/CQDs was evaluated by photodegradation of RhB. Experiment indicated that the introduction of CQDs could improve the photocatalysis activity of BiOI obviously. Moreover, there is a optimum percentage of CQDs. In this photocatalytic system, the enhanced photoactivity was mainly attributed to the heterojunction interface between CQDs and BiOI, as well as the enhanced light harvesting for the appropriate CQDs introduction. The radicals trapping experiments revealed that $O_2^{\bullet-}$, $^{\bullet}OH$ and h^+ were the main active species during the photocatalysis process.

1. Introduction

Nowadays, energy shortage and environmental pollution are the two key issues facing the world.[1–7] Since photocatalysis by semiconductors has been regarded as one of the most efficient ways to resolve water pollution and energy issues, semiconductors emerge in large numbers.[1,4,8–12] Recently, BiOX (X = Cl, Br, I) attracts a lot of attention due to its outstanding performance.[3,10,13,14] Among them, BiOI has obtained much attention because of its strong absorption under visible light irradiation, which would improve the utilization of solar energy.[4,11] Nevertheless, the photocatalytic performance of BiOI is limited by its fast recombination of the photo-excited electron–hole pairs.[4,15,16] In order to resolve this problem, BiOI-base heterojunctions have been designed to improve its photocatalytic activity, which include BiOI/g-C_3N_4,[17,18] BiOI/TiO_2,[19] BiOI/CdS,[20] BiOI/ZnO,[21] BiOI/Bi_2WO_6,[22] BiOI/BiOBr,[23] BiOI/$BiPO_4$,[24] *etc.* However, due to the large-size materials in these hybrid systems, the contact interfaces are insufficient and incompact. Hence, perfect interfaces couldn't be constructed and surface defects would emerge. As a result, the electron–hole pairs would tend to recombine on surface defects and affect the photocatalytic performance. Therefore, to overcome this affect, small size materials could be introduced to BiOI material to construct tight touch interfaces.[25,26]

Carbon quantum dots (CQDs), which is a new kind of carbon materials with size less than 10 nm, has a lot of virtues, such as low cytotoxicity, excellent biocompatibility, chemical inertness, low-cost.[27–31] More importantly, the conjugated π structure of CQDs give it excellent electron transfer/reservoir properties.[26] Recently, a series of CQDs-based materials have been developed, such as CQDs/TiO_2,[32–34] CQDs/g-C_3N_4,[35] CQDs/Bi_2WO_6,[36] and CQDs/BiOBr.[31,37] CQDs/Bi_2MoO_6,[38] CNS/CQDs,[39] CQDs/$Bi_7O_9I_3$,[40] CQDs/PpPD,[41] *etc.* Nevertheless, the study on structure–performance relationship of CQDs-based materials is still relatively insufficient and the photocatalytic mechanism of CQDs-based materials is expected to be investigated further.

Herein, Bi/BiOI/CQDs nano-materials were prepared successfully *via* a facile method. The relationship between structure and properties of the photocatalyst is studied by different techniques. The rhombohedral Bi was found in BiOI/CQDs matrix, which could be transformed from the BiOBr matrix during the growth process of CQDs under high temperature and pressure,[42] and it may exhibit superior surface plasma resonance (SPR) effect in photocatalytic process. To the best of our knowledge, the SPR effect would improve the photocatalytic performance of the photocatalyst.[3,43–45] Bi plays two main roles in photocatalysis. On the one hand, Bi can be used as an electron donor and conductor, promoting the separation of electron–hole pairs. On the other hand, its SPR effect could prompt the photocatalyst to harvest more light absorption.[2,44] However, as far as we know, no existing report is about the synthesis of the Bi/BiOI/CQDs ternary material. Therefore, the photocatalytic performance of Bi/BiOI/CQDs nano-materials is evaluated by photo-degradation of rhodamine (RhB). Finally, a reasonable mechanism of RhB photodegradation by Bi/BiOI/CQDs was proposed based on free radicals trapping experiments.

2. Results and discussion

2.1 Compositional and structural information

The XRD pattern is shown in Fig. 1a. All diffraction peaks of BiOI could be indexed to tetragonal BiOI (JCPDS No.10-0445). As

[a]School of Power and Energy, Northwestern Polytechnical University, Xi'an 710072, China. E-mail: fjf@nwpu.edu.cn

[b]School of Chemistry and Chemical Engineering, Northwestern Polytechnical University, Xi'an 710072, China

† Electronic supplementary information (ESI) available. See DOI: https://doi.org/10.1039/d3ra05145e

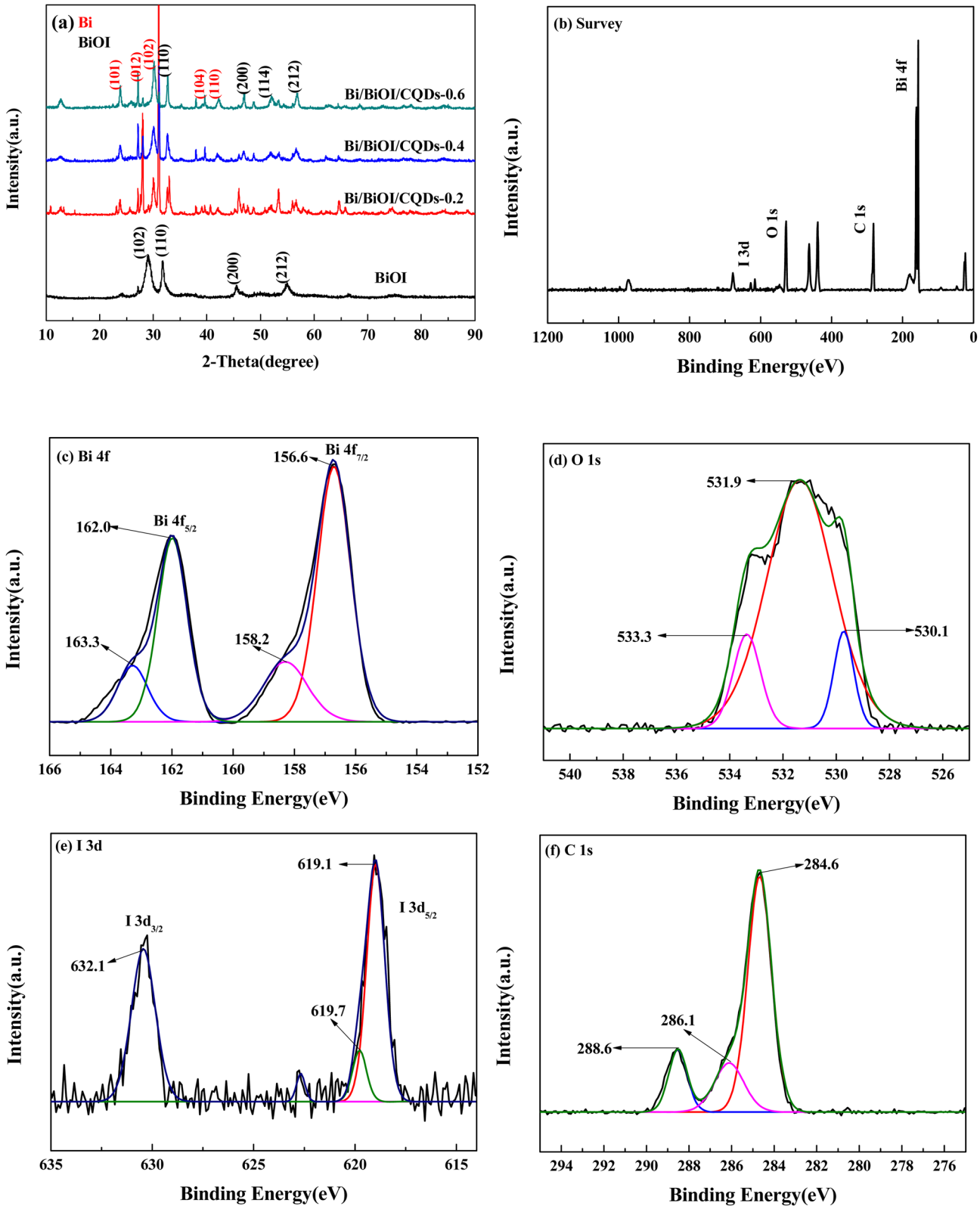

Fig. 1 (a) XRD patterns of Bi/BiOI/CQDs materials, and XPS spectra of Bi/BiOI/CQDs samples. (b) Survey of the sample; (c) Bi 4f; (d) O 1s; (e) I 3d and (f) C 1s.

for Bi/BiOI/CQDs, some new peaks appeared at at 23.9°, 27.2°, 38.0° and 39.6° which could be indexed to the (101), (012), (104) and (110) crystal planes of rhombohedral Bi (JCPDS Card No.44-1246). It should be transformed from the BiOI matrix during the growth process of CQDs under high temperature and pressure, which may exhibit superior surface plasma resonance (SPR)

effect in photocatalytic process.[14,42] Furthermore, the (110), (200), and (212) were shifted to larger angles, which may be attributed to the interaction between BiOI and CQDs.[46] In addition, there are no obvious diffraction peaks of CQDs, which could be explained by its low amount in Bi/BiOI/CQDs materials. Similar result could be found in other systems.[47]

The XPS spectra of BiOI/CQDs samples (Fig. 1b) indicates that Bi/BiOI/CQDs contains Bi, O, and C and I elements. As for the high-resolution spectra of Bi (Fig. 1c), two peaks located at 156.6 and 162.0 eV can be assigned to the Bi $4f_{7/2}$ and Bi $4f_{5/2}$ of Bi^{3+} in Bi/BiOI/CQDs, respectively. Furthermore, the peaks located at 158.2 and 163.3 eV can be attributed to Bi $4f_{7/2}$ and Bi $4f_{5/2}$ of elemental Bi,[46] respectively, which is consistent with the results of XRD. The O 1s spectrum in BiOI (Fig. 1d) can be fitted into three peaks located at 530.1, 531.9 and 533.3 eV (which are attributed to O in the BiOI and other components, such as OH and H_2O). Two peaks located at 619.1 and 632.1 eV (Fig. 1e) can be assigned to the I $3d_{5/2}$ and I $3d_{3/2}$ of I 3d in Bi/BiOI/CQDs, and 619.7 eV is attributed to I–O bond. Fig. 1f displays the high resolution XPS-spectra of the C 1s in samples. The peaks at 284.6, 286.1, 288.6 eV can be attributed to C–C/C=C, oxygenated carbon and nitrous carbon for C 1s in Bi/BiOI/CQDs material, respectively.[48] The XPS analysis indicates that the intimate integration of CQDs and BiOI has been constructed in Bi/BiOI/CQDs materials.

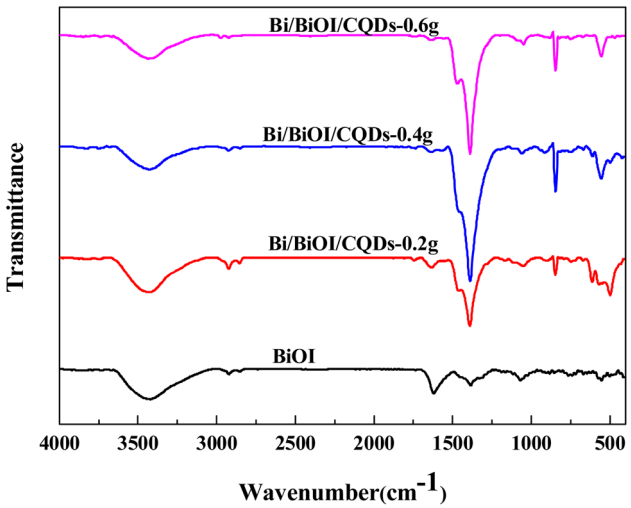

Fig. 2 FTIR spectra of Bi/BiOI/CQDs materials with different CQDs amounts.

Fig. 2 shows the FI-IR spectra of BiOI and Bi/BiOI/CQDs materials with different CQDs loading amounts. The absorption peaks located at 3432 cm^{-1} and 2921 cm^{-1} can be assigned to the stretching vibrations of O–H and C–H. The peak at 1572 cm^{-1} is associated with the C=O stretching vibration whereas the peak at 1466 cm^{-1} is attributed to the absorption peaks of $–COO^-$. These reveal the existence of CQDs. The peak at 493 cm^{-1} is associated with the Bi–O stretching mode in the BiOBr materials.[49] The FT-IR result shows that CQDs and BiOBr had been successfully coupled together which is consistent with the XPS analysis.

2.2 Morphology and microstructure analysis

The SEM and TEM were shown in Fig. 3. Fig. 3a and b are the SEM images of BiOI. It indicates that BiOI has a shape of hollow microsphere-like structure assembled with lots of BiOI nanosheet. TEM images of BiOI (Fig. 3e and f) are in accordance with SEM. Nano-sheets can be found from the edge of sphere-like structure. Fig. 3c and d display SEM images of Bi/BiOI/

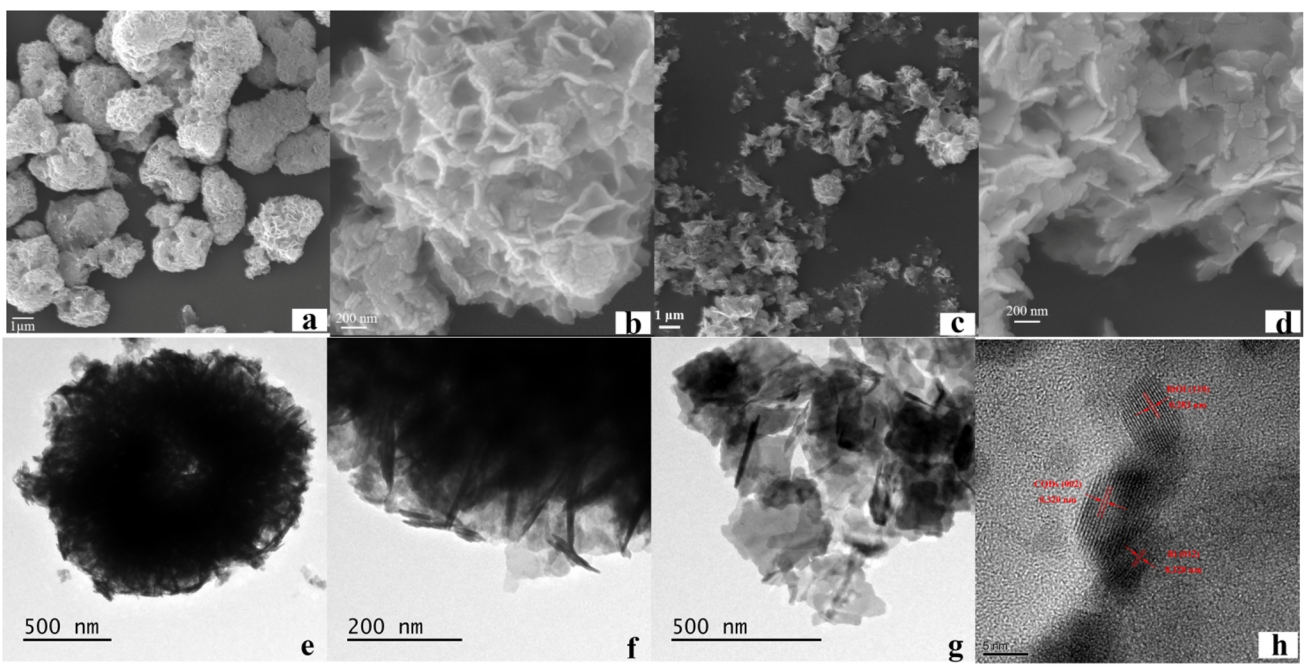

Fig. 3 SEM images of (a and b) BiOI, (c and d) Bi/BiOI/CQDs, TEM images of (e and f) BiOI, and (g and h) Bi/BiOI/CQDs.

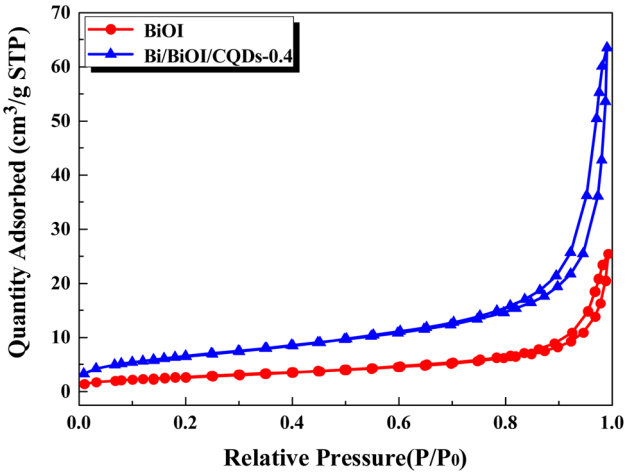

Fig. 4 Nitrogen adsorption–desorption isotherms of the BiOI and Bi/BiOI/CQDs-0.4 materials.

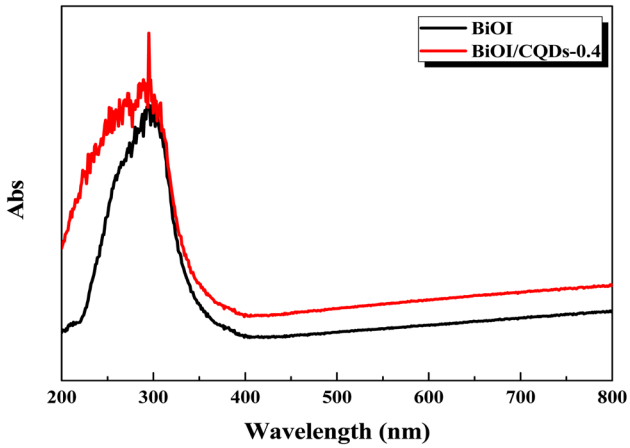

Fig. 5 UV-vis spectra of BiOI and Bi/BiOI/CQDs materials.

CQDs. It can be seen that microsphere collapse after the CQDs is introduced into the BiOI, which may be ascribed to the high temperature and pressure during the grow process of CQDs. At present, BiOI nano-sheets turn into loose aggregations without specific shape (Fig. 3g). High-resolution TEM (HRTEM) image of Bi/BiOI/CQDs (Fig. 3h) shows that the lattice spacing of 0.320 nm, 0.328 nm and 0.282 nm can be observed, which can be attributed to the (002) crystal plane of CQDs,[26] the (012) crystal plane of Bi[26] and the (110) crystal plane of BiOI. It can be observed obviously that several dark dots (CQDs) are dispersed on the surface of BiOI nanosheets (Fig. S2†), which suggests that the CQDs has been modified on the BiOI nanosheets successfully.

The N_2 adsorption–desorption isotherms (Fig. 4) of the BiOI and Bi/BiOI/CQDs-0.4 materials were used to further study their microstructures. The BET surface area of the Bi/BiOI/CQDs-0.4 (24.1518 $m^2\ g^{-1}$) is larger than pure BiOI (9.6596 $m^2\ g^{-1}$). In addition, the BET surface area of Bi/BiOI/CQDs-0.2 and Bi/BiOI/CQDs-0.6 are 10.0151 and 25.3789 $m^2\ g^{-1}$. These data indicate that BET surface areas of the Bi/BiOI/CQDs increase with the increase of CQDs amounts which can be attributed to the formation of the porous structure during the CQDs introduced process. Fig. S3† suggests the existence of mesoporous in the BiOI/CQDs materials which is consistent with the results in the literature.[46] Furthermore, the increased BET surface area of Bi/BiOI/CQDs also benefits from the excellent adsorptive performance of CQDs.[49] It has been widely recognized that a higher BET surface area is advantageous for absorb more active species and reactants on its surface, which thus favors the improvement of photocatalytic performance.[26]

2.3 Optical and electronic properties

Photoabsorption capability is an important factor influencing the photocatalytic performance of photocatalysts,[50] and is usually evaluated by UV-vis diffuse reflectance spectra (DRS). As shown in Fig. 5, the absorption edges of Bi/BiOI/CQDs materials show red shifts compared with BiOI, which means that the optical absorption in visible light is enhanced. The DRS results suggest that CQDs may play an important role in utilizing visible light and such produce more photoexcited e^-–h^+ pairs. The band gap of Bi/BiOI/CQDs materials were estimated *via* the classical Tauc approach. As shown in Fig. 6, the band gap of Bi/BiOI/CQDs materials become smaller than that of BiOI. A narrower band gap means a higher photocatalytic performance in visible light.[26]

Photoluminescence (PL) intensity of photocatalysts is capable of characterizing the recombination efficiency of photogenerated e^- and h^+.[51] As is known, weaker intensity represents lower efficiency of e^- and h^+ recombination.[26] As shown in Fig. 7, all the materials have strong emission peak centered between 370 and 400 nm with an excitation wavelength of 275 nm. Bi/BiOI/CQDs materials display lower PL intensity than that of pure BiOI, indicating the decreasing recombination efficiency of e^- and h^+. This phenomenon can be ascribed to the highly efficient photoexcited carrier transfer ability between the interacted interface of CQDs and BiOI, leading to the effective separation of the e^- and h^+.[49]

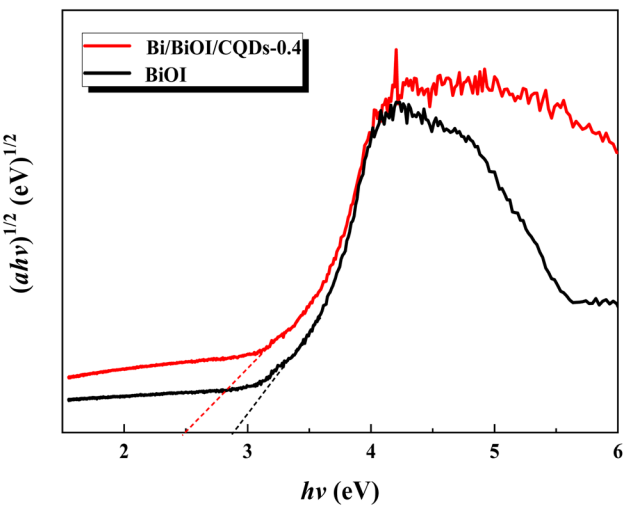

Fig. 6 $(\alpha h\nu)^{1/2}$ *vs.* hν curves of Bi/BiOI/CQDs materials with different contents of CQDs.

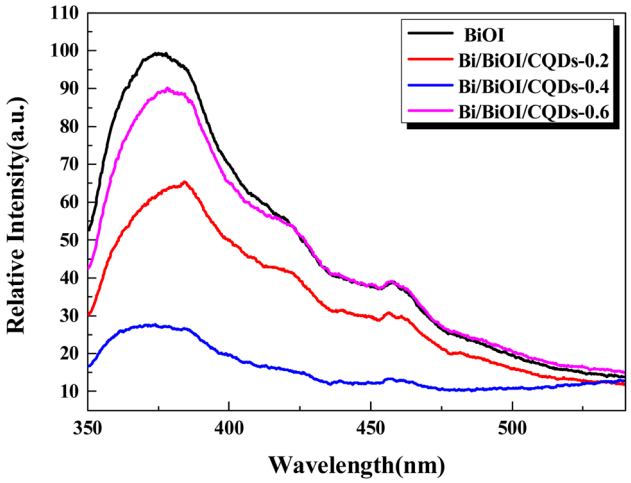

Fig. 7 PL spectra of Bi/BiOI/CQDs hybrid materials with different CQDs amounts.

2.4 Photocatalytic tests

The photocatalytic performance of Bi/BiOI/CQDs with different CQDs was evaluated. The absorption–desorption balances between the catalyst and RhB were achieved in 30 min before photocatalysis. Fig. 8a shows that Bi/BiOI/CQDs samples have much better photocatalytic performance than BiOI. The Bi/BiOI/CQDs-0.4 material displays the best photocatalytic performance. All of the RhB was photodegraded at 105 min. The corresponding fitted Langmuir–Hinshelwood models (Fig. 8b) show that the photodegradation of RhB obeys pseudo-first-order kinetics well. The Bi/BiOI/CQDs-0.4 material has the maximum rate constant of 0.0266 min^{-1}. It indicated that proper introduction of the CQDs is beneficial for the improvement of the photocatalytic performance of BiOI. The photocatalytic performance of Bi/BiOI/CQDs in this work is compared with that of the recent reported Bi-based catalysts (Table S1†). It indicates that Bi/BiOI/CQDs exhibits excellent photocatalytic performance, and the photodegradation efficiency by Bi/BiOI/

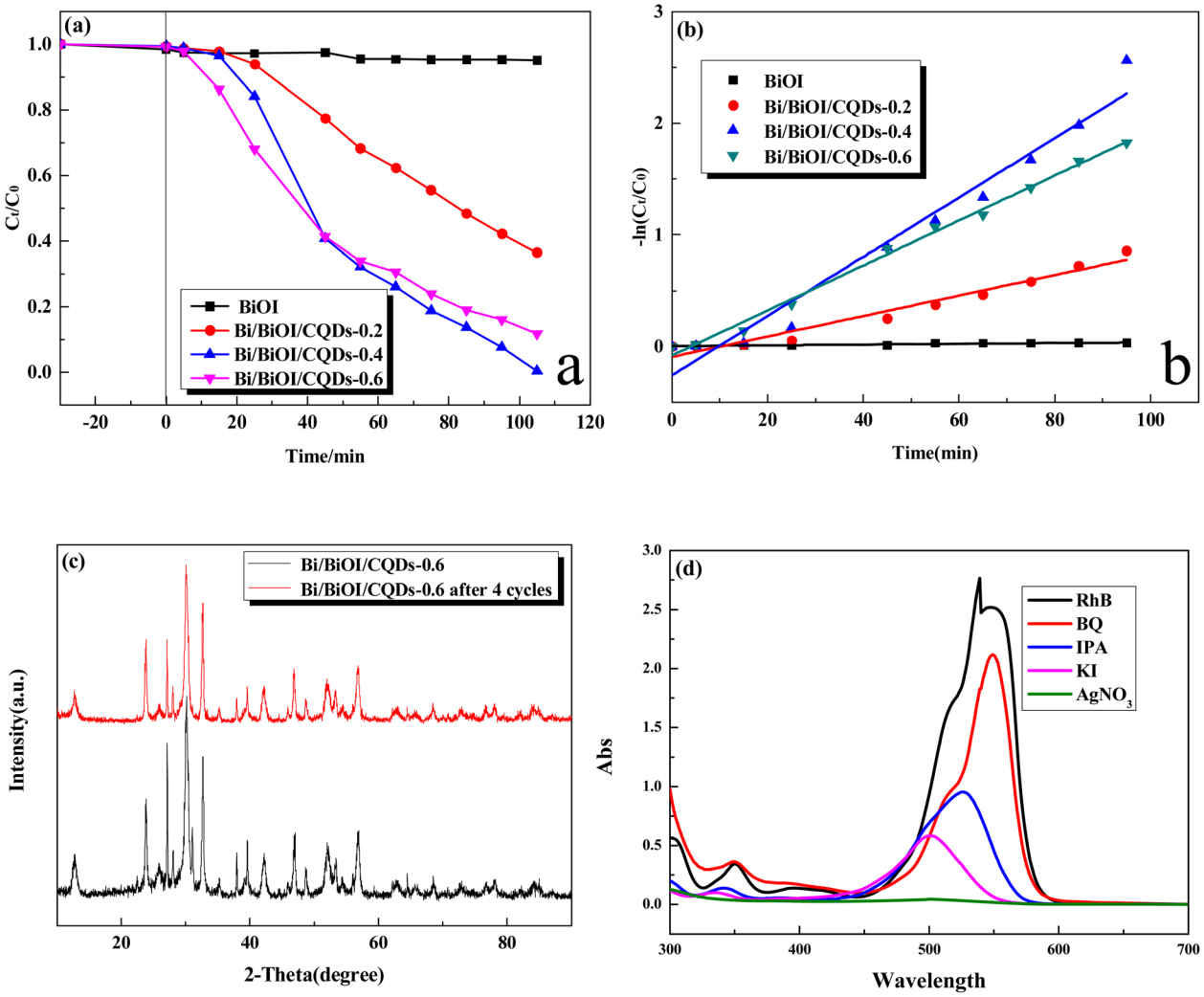

Fig. 8 (a) Photodegradation kinetic curves, (b) fitted Langmuir–Hinshelwood models for degradation of RhB with Bi/BiOI/CQDs materials under visible light irradiation, (c) XRD patterns of the Bi/BiOI/CQDs-0.4 photocatalyst before and after being used for four times. (d) UV-vis absorption spectra of RhB solution in trapping experiments by Bi/BiOI/CQDs materials at 60 min illumination.

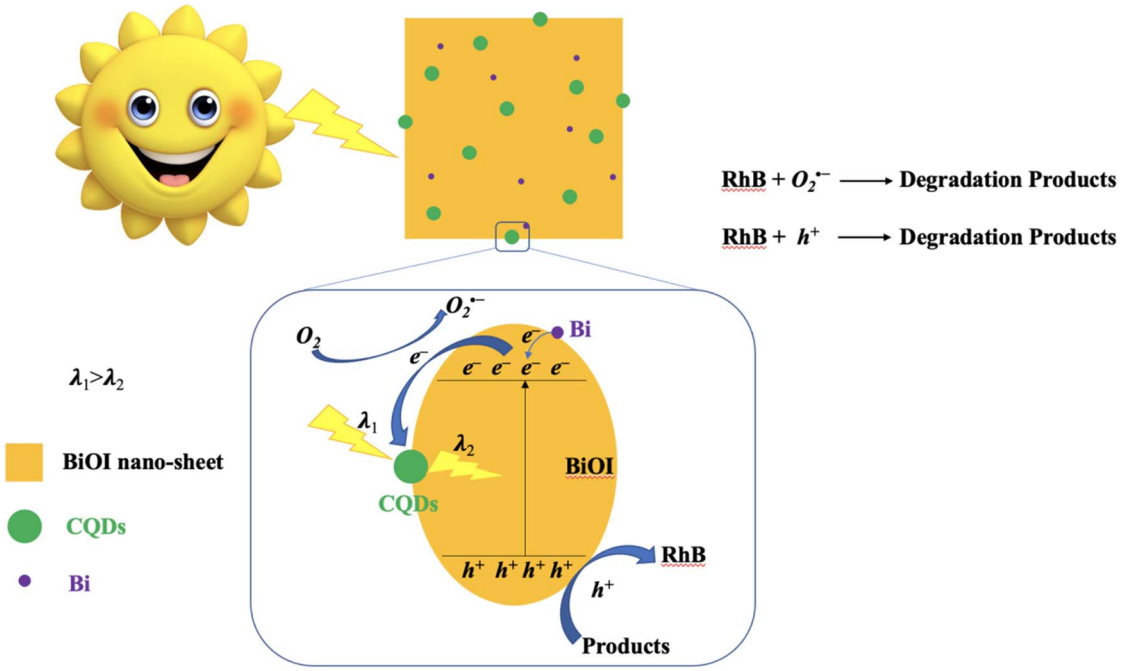

Fig. 9 Schematic of the separation and transfer of photogenerated charges in the Bi/BiOI/CQDs hybrid material combined with the possible reaction mechanism of photocatalytic procedure.

CQDs-0.4 is higher than or is comparable to that reported in the literatures. The stability of the photocatalyst is important for the practical application. XRD spectra (Fig. 8c) indicate that the regenerated photocatalyst exhibits excellent physical stability. Meanwhile, Fig. S4† shows that the photocatalytic performance could still be maintained after four cycles, demonstrating that the Bi/BiOI/CQDs material has high photostability which is in accordance with the result in Fig. 8c.

2.5 Mechanism of pollutant photodegradation

In order to elucidate the photocatalytic mechanism involved in the photodegradation of RhB by Bi/BiOI/CQDs materials, a series of photodegradation experiments with the addition of different scavengers were carried out. The absorption peak value of RhB at 553 nm analyzed by UV-vis spectrophotometer could indirectly reflect the degradation efficiency after being illuminated for 60 min (Fig. 8d). Fig. 3d shows that photodegradation activity decreases by 84.1% when BQ ($O_2^{\bullet-}$ scavenger) rate is added into the degradation system, which indicates that $O_2^{\bullet-}$ radicals play an important role in the photodegradation process. Simultaneously, photodegradation activity decreases by 37.7% and 23.0% when IPA ($^{\bullet}OH$ scavenger) and KI (h^+ scavenger) is added into the degradation system, respectively. It can be seen that the photodegradation was completed at 60 min illumination when $AgNO_3$ (e^- acceptor) is added into the degradation system, demonstrating that e^- does not have direct effect to the photocatalytic process. Therefore, it can be assumed that $O_2^{\bullet-}$ radicals are main active species during the photocatalysis process, while $^{\bullet}OH$ and h^+ plays a secondary and a third role in the photodegradation process, respectively.

Based on the above experimental results, the photocatalytic mechanism diagram of Bi/BiOI/CQDs hybrid materials is proposed in Fig. 9. The enhanced photocatalytic activity of Bi/BiOI/CQDs can be ascribed to the synergistic effects of several factors. Firstly, for the formation of the heterojunction interface among CQDs and BiOI, the photoexcited e^- can transfer from BiOI to CQDs. Moreover, the delocalized conjugated structure of CQDs makes it easier to transfer the photogenerated carriers, resulting in efficient e^-–h^+ pair separation. Secondly, the up-converted PL property of CQDs can convert longer wavelength light to shorter wavelength light, which can in turn excite BiOI to form photoexcited e^-–h^+ pairs.[29] Thus, more e^-–h^+ pairs are excited, result in an enhanced photocatalytic activity. The photoexcited e^- can be captured by O_2 molecules in the system to generate the $O_2^{\bullet-}$ radicals. The generated $O_2^{\bullet-}$ and the h^+ would play important role in the photodegradation process, leading to dramatic photocatalytic performance. Thirdly, Due to the SPR effect of Bi, the visible light adsorption ability is improved which leads to the increased photocatalytic performance of Bi/BiOI/CQDs towards RhB degradation. In addition, both Bi and CQDs serve as electron donor, thus more e^-–h^+ pairs would be produced. Moreover, Bi could also be used as conductor, promoting the efficient separation of e^-–h^+ pairs. Therefore, the photocatalytic activity of Bi/BiOI/CQDs could be enhanced effectively.

3. Conclusion

In summary, a novel Bi/BiOI/CQDs hybrid material was successfully prepared through a facile solvothermal method followed by a hydrothermal process. The CQDs were dispersed

on the surface of microsphere-like BiOI and tight junctions were formed. The photocatalytic activities of Bi/BiOI/CQDs materials on RhB degradation under visible light irradiation increased dramatically. The Bi/BiOI/CQDs-0.4 exhibited the optimal photocatalytic performance for the degradation of RhB. Furthermore, the Bi/BiOI/CQDs materials showed excellent reusability and stability, which was valuable for the potential applications of environmental protection. The enhanced photocatalytic performance of Bi/BiOI/CQDs material was attributed to excellent electron transfer ability and the increased light harvesting capacity of CQDs. The radicals trapping experiments revealed that $O_2^{\bullet-}$ and $^{\bullet}OH$ were the main active species during the photocatalysis process. This work was expectedly to provide appropriate theoretical reference for the new development of CQDs-based hybrid materials with high photocatalytic performance.

Conflicts of interest

There are no conflicts of interest to declare.

Acknowledgements

The authors are grateful for the financial support provided by the Natural Science Basic Research Program of Shaanxi Province (No. 2021JM-056), the Key Research and Development Program of Shaanxi (Grant No. 2021GXLH-01-16), the Science Center for Gas Turbine Project (No. P2022-B-V-003-001), and the Fundamental Research Funds for the Central Universities (No. G2022KY05108).

References

1 H. Kumari, *et al.*, A Review on Photocatalysis Used For Wastewater Treatment: Dye Degradation, *Water, Air, Soil Pollut.*, 2023, **234**(6), 349.

2 W. Li, *et al.*, Pine Dendritic Bi/BiOBr Photocatalyst for Efficient Degradation of Antibiotics, *Langmuir*, 2023, **39**(11), 4140–4149.

3 Y. Quan, *et al.*, Influence of Bi co-catalyst particle size on the photocatalytic activity of BiOI microflowers in Bi/BiOI junctions – A mechanistic study of charge carrier behaviour, *J. Photochem. Photobiol., A*, 2023, 443.

4 M. Arumugam and M. Y. Choi, Recent progress on bismuth oxyiodide (BiOI) photocatalyst for environmental remediation, *J. Ind. Eng. Chem.*, 2020, **81**, 237–268.

5 S. Zheng, *et al.*, Up-converted nitrogen-doped carbon quantum dots to accelerate charge transfer of dibismuth tetraoxide for enhanced full-spectrum photocatalytic activity, *Colloids Surf., A*, 2021, 615.

6 H. Du, *et al.*, Exceptional visible-light photoelectrocatalytic activity of dual Z-scheme Bi@BiOI-Bi(2)O(3)/C(3)N(4) heterojunction for simultaneous remediation of Cr(VI) and phenol, *J. Colloid Interface Sci.*, 2023, **640**, 132–143.

7 W. Sun, *et al.*, Preparation and Photocatalytic Properties of CQDs-Modified 26-Facet Cu/Cu_2O Composites, *Catal. Lett.*, 2023, 1–13.

8 Y. Zhu, *et al.*, Construction of a hollow BiOI/TiO_2/ZIF-8 heterojunction: Enhanced photocatalytic performance for norfloxacin degradation and mechanistic insight, *J. Alloys Compd.*, 2022, 914.

9 Y. Qu, *et al.*, Controllable synthesis of a sponge-like Z-scheme N,S-CQDs/Bi(2)MoO(6)@TiO(2) film with enhanced photocatalytic and antimicrobial activity under visible/NIR light irradiation, *J. Hazard. Mater.*, 2022, **429**, 128310.

10 M. Arumugam, *et al.*, Enhanced photocatalytic activity at multidimensional interface of 1D-Bi(2)S(3)@2D-GO/3D-BiOI ternary nanocomposites for tetracycline degradation under visible-light, *J. Hazard. Mater.*, 2021, **404**(Pt B), 123868.

11 C. Wang, *et al.*, Enhanced photocatalytic antibacterial and degradation performance by n–p type 0D/2D SnO_{2-x}/BiOI photocatalyst under LED light, *Chem. Eng. J.*, 2021, 411.

12 J. Di, *et al.*, Bismuth oxyhalide layered materials for energy and environmental applications, *Nano Energy*, 2017, **41**, 172–192.

13 S. Vinoth, W.-J. Ong and A. Pandikumar, Defect engineering of BiOX (X = Cl, Br, I) based photocatalysts for energy and environmental applications: Current progress and future perspectives, *Coord. Chem. Rev.*, 2022, 464.

14 Q. Li, *et al.*, In situ synthesis of an advanced Z-scheme Bi/BiOI/black TiO_2 heterojunction photocatalysts for efficient visible-light-driven NO purification, *Appl. Surf. Sci.*, 2021, 562.

15 L. Yang, Z. Zhao and Z. Cai, Enhancing visible-light-enhanced photoelectrochemical activity of BiOI microspheres for 4-chlorophenol detection by promoting with Bi surface plasmon resonance (SPR) and multi-walled carbon nanotubes, *SN Appl. Sci.*, 2020, **2**(7), 1–10.

16 Z. Wu, *et al.*, Internal Electric Field Enhancement by the I-Rich Surface of Highly Crystallized BiOI Nanosheets for Boosted Photocatalytic Degradation of Phenol, *Small Struct.*, 2023.

17 N. Tian, *et al.*, Facet-charge-induced coupling dependent interfacial photocharge separation: A case of BiOI/g-C_3N_4 p–n junction, *Appl. Catal., B*, 2020, 267.

18 X. Zhang, *et al.*, Room-temperature solid phase surface engineering of BiOI sheets stacking g-C_3N_4 boosts photocatalytic reduction of Cr(VI), *Green Energy Environ.*, 2022, **7**(1), 66–74.

19 Y. Zhang, *et al.*, TiO_2/BiOI p–n junction-decorated carbon fibers as weavable photocatalyst with UV-vis photoresponsive for efficiently degrading various pollutants, *Chem. Eng. J.*, 2021, 415.

20 D. Dai, *et al.*, Interspersing CdS nanodots into iodine vacancy-rich BiOI sphere for photocatalytic lignin valorization, *Int. J. Biol. Macromol.*, 2023, **227**, 1317–1324.

21 C. Zhang, *et al.*, p–n Heterojunction of BiOI/ZnO nanorod arrays for piezo-photocatalytic degradation of bisphenol A in water, *J. Hazard. Mater.*, 2020, **399**, 123109.

22 X. Huang, *et al.*, Study on photocatalytic degradation of phenol by BiOI/Bi_2WO_6 layered heterojunction synthesized by hydrothermal method, *J. Mol. Liq.*, 2021, 322.

23 K. Gao, *et al.*, Boosting Photocatalytic Nitrogen Fixation *via* In Situ Constructing Bi Metal Active Sites over BiOBr/BiOI Heterojunction, *Sol. RRL*, 2022, **6**(12), 1–13.

24 O. Amiri, *et al.*, Hierarchical p-BiOI/n-$BiPO_4$ heterojunction nanocomposite with enhanced visible-light photocatalytic desulfurization of thiophene under mild conditions, *Int. J. Hydrogen Energy*, 2021, **46**(9), 6547–6560.

25 J. Di, *et al.*, Carbon quantum dots *in situ* coupling to bismuth oxyiodide *via* reactable ionic liquid with enhanced photocatalytic molecular oxygen activation performance, *Carbon*, 2016, **98**, 613–623.

26 J. Di, *et al.*, Novel visible-light-driven CQDs/Bi_2WO_6 hybrid materials with enhanced photocatalytic activity toward organic pollutants degradation and mechanism insight, *Appl. Catal., B*, 2015, **168–169**, 51–61.

27 X. Hu, *et al.*, Construction of Carbon Dot-Modified g-C_3N_4/$BiOIO_3$ Z-Scheme Heterojunction for Boosting Photocatalytic CO_2 Reduction under Full Spectrum Light, *ACS Sustain. Chem. Eng.*, 2022, **10**(34), 11143–11153.

28 M. Li, *et al.*, Controlling the up-conversion photoluminescence property of carbon quantum dots (CQDs) by modifying its surface functional groups for enhanced photocatalytic performance of CQDs/$BiVO_4$ under a broad-spectrum irradiation, *Res. Chem. Intermed.*, 2021, **47**(8), 3469–3485.

29 S. Y. Lim, W. Shen and Z. Gao, Carbon quantum dots and their applications, *Chem. Soc. Rev.*, 2015, **44**(1), 362–381.

30 G. M. Alshammari, *et al.*, Development of luminescence carbon quantum dots for metal ions detection and photocatalytic degradation of organic dyes from aqueous media, *Environ. Res.*, 2023, **226**, 115661.

31 C. Chuaicham, *et al.*, Efficient photocatalytic degradation of emerging ciprofloxacin under visible light irradiation using BiOBr/carbon quantum dot/saponite composite, *Environ. Res.*, 2022, **212**(Pt E), 113635.

32 X. Wang, *et al.*, Facet-dependent photocatalytic and photoelectric properties of CQDs/TiO_2 composites under visible irradiation, *J. Alloys Compd.*, 2022, 920.

33 B. Zhao, *et al.*, Visible-light-driven CQDs/TiO(2) photocatalytic simultaneous removal of Cr(VI) and organics: Cooperative reaction, kinetics and mechanism, *Chemosphere*, 2022, **307**(2), 135897.

34 S. Tong, *et al.*, Preparation of carbon quantum dots/TiO_2 composite and application for enhanced photodegradation of rhodamine B, *Colloids Surf., A*, 2022, 648.

35 C. Zhao, *et al.*, Carbon quantum dots modified tubular g-C(3) N(4) with enhanced photocatalytic activity for carbamazepine elimination: Mechanisms, degradation pathway and DFT calculation, *J. Hazard. Mater.*, 2020, **381**, 120957.

36 X. Qian, *et al.*, Carbon quantum dots decorated Bi_2WO_6 nanocomposite with enhanced photocatalytic oxidation activity for VOCs, *Appl. Catal., B*, 2016, **193**, 16–21.

37 H. Yu, *et al.*, Enhanced photocatalytic tetracycline degradation using N-CQDs/OV-BiOBr composites: Unraveling the complementary effects between N-CQDs and oxygen vacancy, *Chem. Eng. J.*, 2020, 402.

38 Y. Zhang, *et al.*, Synthesis and testing of carbon quantum dots loaded 2D Bi_2MoO_6 for efficient Hg0 photocatalytic removal, *Appl. Surf. Sci.*, 2023, 633.

39 Y. Wang, *et al.*, In-situ one-step synthesis of porous monolayer carbon nitride nanosheets doped with carbon quantum dots for photocatalytic degradation of Meloxicam, *Colloids Surf., A*, 2022, 647.

40 L. Zhu, D. Shen and K. Hong Luo, Lignin-derived carbon quantum dots-decorated $Bi_7O_9I_3$ nanosheets with enhanced photocatalytic performance: Synergism of electron transfer acceleration and molecular oxygen activation, *Appl. Surf. Sci.*, 2023, 608.

41 Y. Yang, *et al.*, Microwave melting rapid synthesis of CQDs/PpPD heterojunctions with efficient microwave electrodeless lamp photocatalytic performance, *Mater. Today Sustain.*, 2023, **21**, 1–10.

42 W. Li, C. Zhao and Q. Zhang, Synthesis of Bi/BiOCl-TiO_2-CQDs quaternary photocatalyst with enhanced visible-light photoactivity and fast charge migration, *Catal. Commun.*, 2018, **107**, 74–77.

43 R. Wang, *et al.*, Bi spheres decorated g-C3N4/BiOI Z-scheme heterojunction with SPR effect for efficient photocatalytic removal elemental mercury, *Appl. Surf. Sci.*, 2021, 556.

44 M. Wu, *et al.*, Preparation of Bi/BiOBr sensitized titania nanorod arrays *via* a one-pot solvothermal method and construction of kanamycin photoelectrochemical aptasensors, *Dalton Trans.*, 2022, **51**(21), 8279–8289.

45 X. Zhang, *et al.*, The role of Sn in enhancing the visible-light photocatalytic activity of hollow hierarchical microspheres of the Bi/BiOBr heterojunction, *Phys. Chem. Chem. Phys.*, 2015, **17**(12), 8078–8086.

46 C. Zhao, *et al.*, Synthesis of BiOBr/carbon quantum dots microspheres with enhanced photoactivity and photostability under visible light irradiation, *Appl. Catal., A*, 2016, **527**, 127–136.

47 J. Di, *et al.*, Carbon Quantum Dots Modified BiOCl Ultrathin Nanosheets with Enhanced Molecular Oxygen Activation Ability for Broad Spectrum Photocatalytic Properties and Mechanism Insight, *ACS Appl. Mater. Interfaces*, 2015, **7**(36), 20111–20123.

48 S. Zhu, *et al.*, Highly photoluminescent carbon dots for multicolor patterning, sensors, and bioimaging, *Angew Chem. Int. Ed. Engl.*, 2013, **52**(14), 3953–3957.

49 J. Di, *et al.*, Nitrogen-Doped Carbon Quantum Dots/BiOBr Ultrathin Nanosheets: *In Situ* Strong Coupling and Improved Molecular Oxygen Activation Ability under Visible Light Irradiation, *ACS Sustain. Chem. Eng.*, 2015, **4**(1), 136–146.

50 W. Li, *et al.*, Construction of Core-shell Sb(2) s(3) @Cds Nanorod with Enhanced Heterointerface Interaction for Chromium-Containing Wastewater Treatment, *Small*, 2023, e2302737.

51 W. Li, *et al.*, Synergistic Electric Metal (Ni SAs)-Semiconductor (CdS NPs) Interaction for Improved H_2O-to-H_2 Conversion Performance under Simulated Sunlight, *Sol. RRL*, 2023, **7**(10), 1–10.